Highly Active Pt-Co/C Nanoparticles: Controllable Preparation and Catalytic Performance for Methanol Electro-oxidation

Yiqi Cui[1], Shuaikang Ying[2], Hongzhong Cai[3], Yan Wei[3,*], Changyi Hu[3,*]

[1] Faculty of Resource Engineering, Kunming University of Science and Technology, Kunming 650093, China
[2] City college, Kunming University of Science and Technology,
Kunming 650093, China;
[3] State Key Laboratory of Advanced Technologies for Comprehensive Utilization of Platinum Metals, Kunming Insitute of Precious Metals, Kunming 650106, China
*E-mail: weiyan@ipm.com.cn (Yan Wei) and hcy@ipm.com.cn (Changyi Hu)

Carbon-supported platinum (Pt) for oxygen reduction reaction plays an important role in the operation of direct methanol fuel cells (DMFCs). However, complete oxidation of ethanol is difficult due to the low chemical activity of Pt / C. Herein, novel highly active Pt-Co/C nanoparticles with controllable chemical composition and particle size are prepared via a thermal reduction method. The results revealed that the catalyst (particle size: 2–4 nm) is characterized by a good size monodispersity, and exhibits satisfactory chemical activity. The nanoparticles were also characterized by an accurate and maintained stoichiometry ratio, resulting in improved electrocatalytic activity and anti-poisoning ability of the carbon-supported Pt.

1. INTRODUCTION

Carbon-supported platinum (Pt) represents one of the most important development direction of direct methanol fuel cells (DMFCs) due to its high catalytic activity [1]. However, its scarcity and susceptibility to carbon monoxide (CO) poisoning have limited the development of Pt in the catalytic field [2]. The modification of Pt still poses a significant scientific challenge to the development of DMFCs [3, 4].

Previous studies have shown that the catalytic activity of carbon-supported Pt can be rationalized in terms of the energy of the d-band center (εd) [5–8]. The proposed model focuses on the shift of the d-band center in relation to increasing or decreasing the reactivity of carbon-supported Pt catalysts. This is based on a general principle regarding the formation of chemical bonds at a surface:

strong bonding occurs if anti-bonding states are shifted up through the Fermi level (and become empty). The opposite occurs if anti-bonding states are shifted down through the Fermi level (and become filled). Moreover, carbon-supported Pt coatings and doping modifications have also been investigated, such as with amorphous graphene [9], titanium dioxide [10], nickel [11], and ruthenium [12]. Improved catalytic activity and anti-poisoning ability of the modified carbon-supported Pt was achieved in those cases. Most importantly, Zhang et al. [13] suggested that carbon-supported Pt nanoparticles with uniform and fine dispersivity exhibit satisfactory catalytic activity. The above experimental findings indicate that good catalytic activity properties can be obtained through appropriate selection of doping materials and reduction of the nanoparticle size [14, 15]. In addition to its natural abundance, cobalt (Co) is characterized by its good catalytic activity and chemical corrosion resistance.[16–18].

In this work, Co is employed for the doping modification of carbon-supported Pt. The special electronic structure of Co can yield an improved anti-toxic effect and a reduction in the d-band center of carbon-supported Pt [19, 20]. The influence of the doping modification on the crystal structure, particle morphology, catalysis performance, and the anti-toxic effect is systematically investigated. The results of this work may prove useful in meeting the energy requirements for future electric vehicles and other energy-demanding devices.

2. MATERIALS AND METHODS

2.1. Materials and preparation

Acetoacetone platinum (80%), cobalt acetate (97%), 1,2-tetradecanediol ($C_{14}H_{30}O_2$, 90%), o-dichlorobenzene ($C_6H_4Cl_2$, AR), oleic acid ($CH(CH_2)_7COOH$, AR), oleylamine ($C_{18}H_{37}N$, 80-90%), diphenyl ether ($C_{12}H_{10}O$, ≥99.9% (GC)), carbon mesopor (AR), and ethanol (C_2H_6O, AR) were purchased from Aladdin (Shanghai, China).

Pt_3Co/C, $PtCo/C$, and $PtCo_3/C$ were prepared as follows: a) 60 mg of platinum acetoacetone, 12.3 mg/ 36.8 mg/ 10.3 mg of acetic acid diamond, and 43 mg of 1,2-tetradecanediol, 0.6 mL of o-dichlorobenzene, 0.2 mL of oil acid, 0.2 mL of oleylamine and 15 mL of diphenyl were added to a three-necked flask containing ether; b) a collector-type magnetic heating stirrer was used for the co-reduction reaction. The temperature was adjusted to 80 °C with aeration gas (i.e., nitrogen (N_2)), and then incubated for 30 min in order to remove the water from the sample. Afterward, (126.8 mg/ 150 mg/ 219.6 mg) carbon mesopor was added, and the temperature was raised under the stirring of a glass rod. After the temperature reached 220 °C, the temperature was maintained for 1 h to ensure that the reaction was completed. c) The sample was placed in ethanol, and suction filtration was then performed. The sample was then placed in a vacuum drying box and dried for 12 h at 60 °C under vacuum. d) The dried samples were treated at 250 °C for 60 min under N_2; e) These samples were then processed at 400 °C for 4 h under $N_2 + H_2$ ($N_2:H_2 = 2:1$). After the heat treatment was completed, the samples were left to cool in the furnace.

2.2. Characterization

The microstructure was characterized by means of field-emission scanning electron microscopy (FESEM; TESCAN VEGA3) and transmission electron microscopy (TEM; Tecnai G2 20 STWIN) performed at 5 kV and 160 kV, respectively. The phase structure was determined via X-ray diffraction (XRD; D/Max-2200) performed at 30 kV and 30 mA using Cu-Kα radiation (λ=0.15406 nm) for 2θ ranging from 20° to 90°. The surface chemical state of the product was evaluated by means of X-ray photoelectron spectroscopy (XPS; PHI5000 Versaprobe-II ULVACPHI) employing Al-Kα radiation.

2.3. Preparation of the working electrode

The working electrode was prepared in accordance with a previously reported procedure. Typically, the catalyst dispersion was prepared by mixing 8 mg of catalyst in 2.5 mL of solution containing 2.4 mL of ethanol and 100 µL of 5 wt.% Nafion solution. This mixture was then subjected to 30 min of ultrasonication. A glassy carbon (GC) GC disk electrode (diameter: 5 mm) served as the substrate for the support. Prior to use, the GC electrode was polished using aqueous alumina suspension on felt polishing pads. Afterward, the catalyst suspension was pipetted (by means of micropipetting) on the GC surface, leading to a catalyst loading of ~0.2 mg/cm^2 for each catalyst. The working electrode was dried under N$_2$ flow at room temperature.

2.4. Electrochemical tests

The electrochemical performances were assessed using an electrochemical workstation (CHI760E) and a three-electrode system. This system consisted of a glassy carbon (GC) electrode, Pt plate counter electrode, and saturated calomel electrode (SCE) which is separated from the working electrode compartment by a closed electrolyte bridge.

The catalyst performance in the room-temperature oxygen reduction reaction (ORR) was evaluated in HClO$_4$ electrolyte solution (0.1 mol/L) using a glass carbon rotating disk electrode (RDE) at a rotation speed of 1600 rpm. Negative-going linear sweep voltammograms were recorded from 1.2 V to 0 V at 100 mV·s^{-1} and room temperature in the presence of bubbling ultra-pure oxygen to maintain a saturated oxygen atmosphere near the working electrode. For the ORR polarization curve, the current density was normalized with reference to the ECSA to obtain the specific activities.

The catalyst performance in the room-temperature methanol oxidation reaction (MOR) was also measured by means of cyclic voltammetry. For these measurements, a potential window of 0 V to 1.5 V was scanned at 100 mV·s^{-1} until a stable response was obtained, and the voltammograms were then recorded. An aqueous solution of 0.1 mol/L HClO$_4$ with 2.0 mo1/L CH$_3$OH was used as the electrolyte. For each catalyst, the specific activity was obtained by normalizing the current density by the corresponding ECSA. The electrolyte solutions were purged with high-purity N$_2$ gas for 30 min to reduce the level of oxygen dissolved prior to each cyclic voltammetry measurement, and the solution kept under N$_2$ flow. In addition, a chronoamperometry curve was measured at a constant potential of -0.5 V under ambient conditions.

To ensure O_2 saturation during the linear sweep voltammetry (LSV) measurement, O_2 was passed through the electrolyte. The measurements were performed at a scan rate of $5\,mV\,s^{-1}$ with $HClO_4$ solution (0.1 mol/L) as the electrolyte.

3. RESULTS AND DISCUSSION

3.1. Microstructure

In general, the smaller nanoparticles exhibited better chemical activity than the larger nanoparticles. Fig. 1 shows TEM images and grain distributions of the Pt_3Co/C, $PtCo/C$, and $PtCo_3/C$. As shown in the figure, the samples consist of nearly spherical uniformly sized grains (grain radii of 2.30, 1.98, and 1.78 nm observed for Pt_3Co/C, $PtCo/C$, and $PtCo_3/C$, respectively). The TEM image in Fig. 1c shows that, compared with Pt_3Co/C and $PtCo/C$, $PtCo_3/C$ is characterized by a better dispersion and a smaller nanoparticle size. That is, Co can reduce the surface energy during nanoparticle growth, thereby preventing the agglomeration and growth of nanoparticles [21, 22].
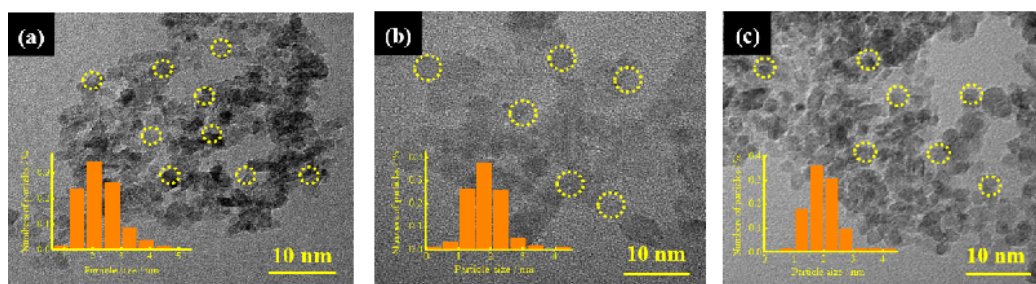

Figure 1. TEM images and grain size distribution of the samples (a) Pt_3Co/C; (b) $PtCo/C$; (c) $PtCo_3/C$.

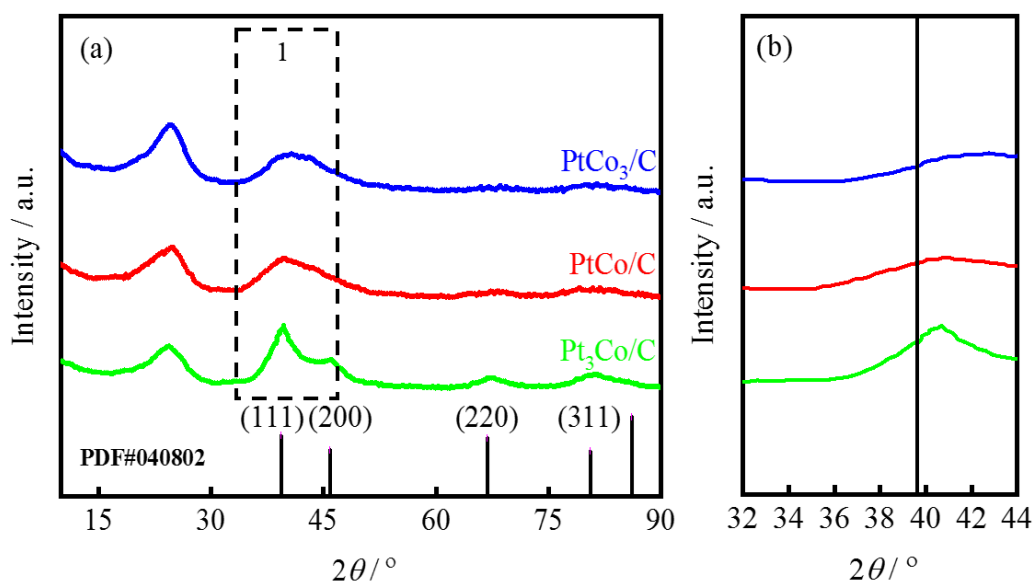### 3.2. Phase composition and valence states of the elements

Figure 2. XRD patterns of (a) Pt_3Co/C, $PtCo/C$, and $PtCo_3/C$ samples; (b) magnified view of area 1 shown in Fig. 2a.

Fig. 2 shows the XRD patterns of the as-prepared Pt_3Co/C, $PtCo/C$, and $PtCo_3/C$. The diffraction peak of Pt (PDF#040802) occurs for all three samples, verifying that the nanoparticle is composed of Pt [23]. Compared with those of Pt_3Co/C, the diffraction peaks gradually shift to higher 2θ values as the Co composition in the Pt–Co nanoparticle increases (Fig. 2b). This can be attributed to a decrease in the lattice distance when smaller Co atoms replace Pt atoms in the lattice [24]. Notably, a diffraction peak, which could be indexed as the (002) crystal planes of graphite (PDF#41-1487) [25], occurs for all three samples.

The chemical composition of Pt_3Co/C, $PtCo/C$, and $PtCo_3/C$ is investigated further via XPS (see Fig. 3). The evidence presented in Figs. 1 and 2 suggests that the nanoparticles are composed of Pt, Co, and C, as indicated in Fig. 3a. The binding energy scale was corrected based on the C1s peak (~284.8 eV) as a standard of the internal binding energy [26]. Notably, the $Pt4f_{7/2}$ peak is characterized by multiple pairs of overlapping peaks, attributable to $Pt_{4f7/2}$ and $Pt_{4f5/2}$, of metallic Pt species. The other two pairs of peaks correspond to Pt^{2+} species. Some Pt^{2+} may have resulted from incomplete restoration during the co-restore reaction.
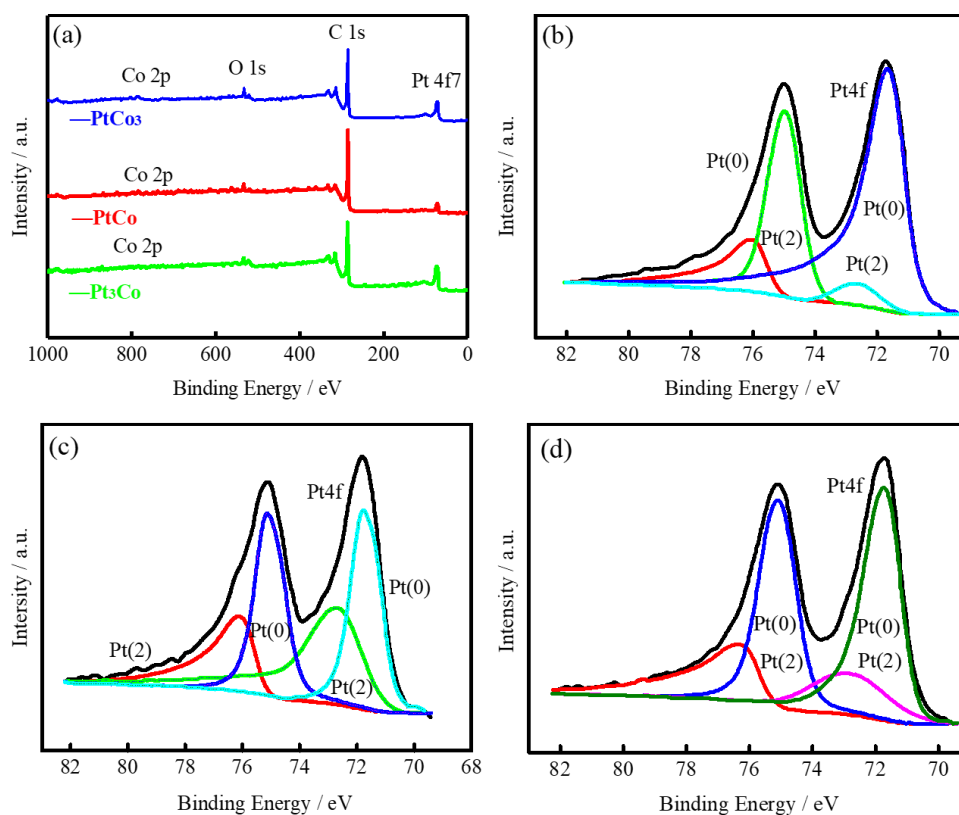

Figure 3. X-ray photoelectron spectroscopy (XPS) scan results of the samples (a) survey spectrum and $Pt4f_{7/2}$; (b) Pt_3Co/C; (c) $PtCo/C$; (d) $PtCo_3/C$.

Importantly, the $Pt4f$ binding energy of the Pt-Co/C nanoparticles is blue-shifted compared with that of Pt. For example, the $Pt4f_{7/2}$ of Pt_3Co/C, $PtCo/C$, and $PtCo_3/C$ occurs at binding energies of 71.5, 71.6, and 71.7 eV, respectively [27]. This is due to the fact that the electronic structure of Pt is mainly affected by Co, which induces the lattice compression strain of Pt. The consequent blue-

shifting of the Pt4f binding energy results in improved catalytic activity of the catalyst. The binding energy is strongly correlated with the adsorption/desorption capability of reaction species on the catalyst surface, consistent with the d-band center of the Pt-Co/C nanoparticles [28].

Table 1 shows the test results of Pt4$f_{7/2}$ and Pt4$f_{5/2}$ corresponding to Pt-Co/C nanoparticles with different Pt:Co molar ratios. The electronic binding energy is basically unchanged for Pt4$f_{7/2}$ in Pt$_3$Co/C, PtCo/C, and PtCo$_3$/C, but drops to 75.00–74.96 eV for Pt4$f_{5/2}$. The decrease in the electronic binding energy of Pt4$f_{5/2}$ results partly from the fact that the graphitization degree of the carbon support in the Pt$_3$Co/C, PtCo/C, and PtCo$_3$/C catalysts has been reduced. Consequently, the electronic interaction between Pt and C is weakened. However, due to the electronegativity difference between Pt and Co, the electrons are transferred from Co with low electronegativity to Pt with high electronegativity, thereby reducing the adsorption energy of the Pt-Co bond [29, 30].

Table 1. XPS spectroscopic data of the samples shown in Figure 3.

Sample	Pt4$f_{7/2}$	Pt4$f_{5/2}$
Pt/C [31]	71.60	75.00
Pt$_3$Co/C	71.59	74.96
PtCo/C	71.60	74.96
PtCo$_3$/C	71.59	74.98

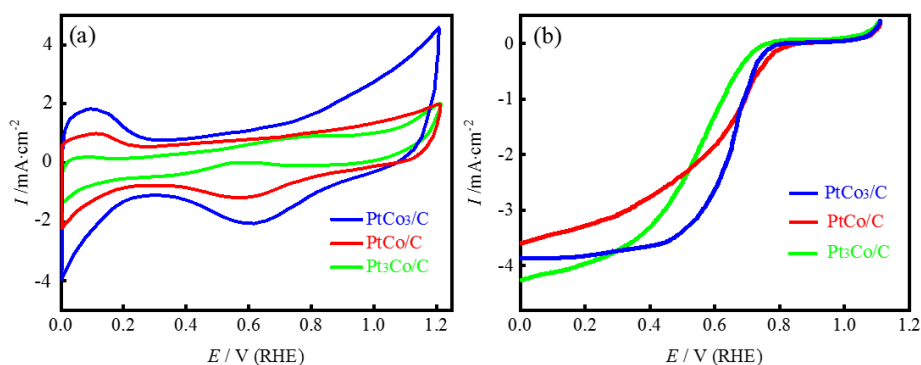*3.3. Electrocatalytic activity of anode methanol oxidation*

Figure 4. The (a) CV (scanning rate: 100 mV/s) curves and (b) LSV (scanning rate: 5 mV/s) curves of the samples in 0.1 mol/L HCIO$_4$ at 25°C.

The catalyst performance in the oxygen reduction reaction (ORR) is also investigated by means of cyclic voltammetry (CV) and linear sweep voltammetry (LSV), as shown in Fig. 4. Significant Pt electrochemical characteristic peaks are observed in Fig. 4a. Furthermore, Fig.4a also reveals half-wave potential (E$_{1/2}$) values of 0.5 V, 0.55 V, and 0.6 V for Pt$_3$Co/C, PtCo/C, and PtCo$_3$/C, respectively. Besides, the CV test performed on the PtCo/C nanoparticles shows that the current density increases with increasing Co content. The highest current density (4.2 mA/cm^2), which is obtained for the PtCo$_3$/C catalyst, is 0.6 and 0.4 times higher than those of the Pt$_3$Co/C and PtCo/C catalysts, respectively. More importantly, it can also be found that the catalytic activity of PtCo/C

nanoparticles enhances with increasing Co content according to cyclic voltammetry (CV) and linear sweep voltammetry (LSV) experiments. These results suggest that the electrochemical activity of $PtCo_3/C$ has been significantly increased [32].

The PtCo/C nanoparticle methanol oxidation reaction (MOR) is investigated by measuring the CV profiles of Pt_3Co/C, PtCo/C, and $PtCo_3/C$ in $HClO_4$+2.0 mo1/L CH_3OH, as shown in Fig. 5. The high cathodic peak current density (of the density values obtained) can be used to evaluate the catalytic activity of the PtCo/C nanoparticle, and comparable peak current densities imply good electrocatalytic activity [33]. As shown in the profiles, methanol oxidation of Pt_3Co/C, PtCo/C, and $PtCo_3/C$ occurs at current densities of 28.34 mA/cm^2, 43.50 mA/cm^2, and 65.34 mA/cm^2, respectively. $PtCo_3/C$ exhibits the best activity due to its high content of Co that can reduce the d-band center and improve the catalytic activity [28]. In addition, compared with Pt_3Co/C and PtCo/C, $PtCo_3/C$ is characterized by a smaller average particle size and, hence, contains more active sites [34]. The anodic peaks shift to lower potential with increasing Pt:Co molar ratio. Under low potential, oxygen species are easily generated by Co. The oxygen species can oxidize the CO molecules adsorbed on the surface of the Pt atom, thereby improving the resistance of the Pt-Co/C nanoparticles to CO poisoning. In addition, compared with the other two catalysts, the $PtCo_3/C$ catalyst exhibits better catalytic activity for methanol oxidation, owing possibly to the strong electronic interaction between the Pt and Co interface [35].
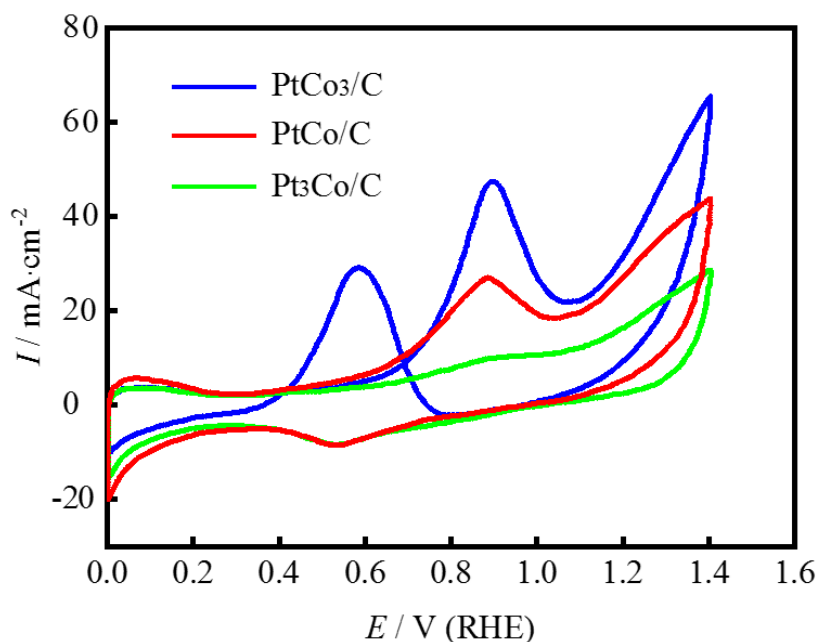

Figure 5. The CV curves (scanning rate: 100 mV/s) of the samples in 0.1 mol/L $HClO_4$ with 2.0 mo1/L CH3OH aqueous solution at 25°C.

The anti-poisoning ability of the catalyst is generally expressed in terms of the I_f/I_b value. The occurrence of a positive peak (I_f) indicates the oxidation potential of methanol and the occurrence of the reverse peak (I_b) indicates the oxidation of the carbon-containing intermediate generated in the forward sweep process [36]. The I_f/I_b value increases with increasing anti-poisoning ability of the

catalyst. The doped Co is easily oxidized in the air and, hence, the I_f/I_b value increases with increasing molar ratio of Co:Pt, as shown in Table 2. During the reaction, the oxidized Co on the surface of the PtCo/C nanoparticles can adsorb (to a certain extent) the intermediate-product CO oxidized by methanol. This results in oxidation of the product to carbon dioxide, leading to an increase in the amount of Pt released. The active site participates in the process of adsorption and oxidation of methanol, thereby improving the catalytic performance and anti-poisoning performance of the PtCo/C nanoparticles [35].

Table 2. I_f/I_b values of the samples considered in Figure 5

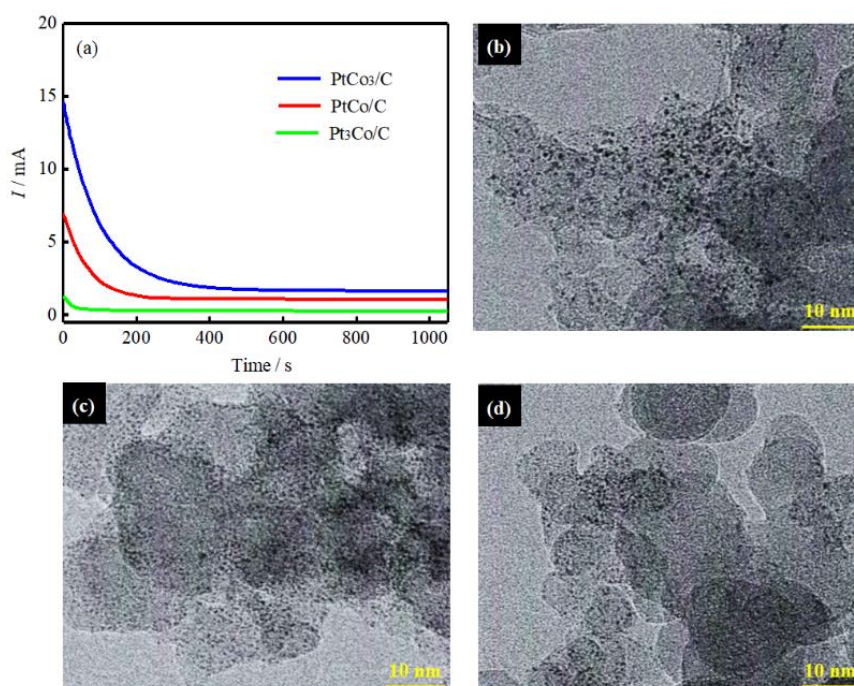| Sample	I_f/I_b
Pt/C [37]	5.2
Pt_3Co/C	9.5
PtCo/C	15.2
$PtCo_3/C$	23.5

Figure 6. Chronoamperometric curves and changes in the morphology of the samples after testing in 0.1 mol/L $HClO_4$ with 2.0 mol/L CH_3OH aqueous solution at 25°C and a potential of 0.5 V (a) chronoamperometric curves of the samples; changes in the morphology of Pt_3Co/C (b), PtCo/C (c), and $PtCo_3/C$ (d).

The methanol oxidation current of the PtCo/C nanoparticles was measured by means of chronoamperometry, as shown in Fig. 6. These results reveal that the $PtCo_3/C$ catalyst is highly stable, with the catalytic activity retained for numerous consecutive runs. After the chronoamperometry test, the morphology and good dispersion of the PtCo/C nanoparticles remain almost unchanged.

Combining the above evidence with the results of the present study confirms that increasing the Co content of the nanoparticles leads to significant enhancement of the catalytic activity and anti-toxicity [15].

The catalytic activity of the PtCo/C nanoparticles prepared in this work was considerably larger than that of other similar catalysts, as shown in Table 3. The specific activity (j_s) and I_f/I_b of the catalyst in the present work are superior to those of the catalysts reported in the literatures, indicating the remarkable catalytic capability of the PtCo/C nanoparticles for methanol.

Table 3. Specific activity (j_s) and I_f/I_b of the catalyst for methanol obtained via different methods.

the type of catalysts	j_s (mA cm^{-2})	I_f/I_b
Pt/C [37]	11.62	5.2
PtRu/C [38]	25.71	18.1
Pt/ TiO$_2$-C [39]	14.33	15.4
This work	65.34	23.5

4. CONCLUSIONS

1) PtCo/C nanoparticle catalysts with different molar ratios are prepared by means of a reduction method. The catalysts can be listed as follows, PtCo$_3$/C>PtCo/C>Pt$_3$Co/C, i.e., in descending order of catalytic activity for methanol oxidation. With increasing Co content, the anti-poisoning performance of the catalyst is enhanced.

2) Through the aforementioned reduction method, nanoparticles with a particle size of 2–4 nm, good monodispersion, and uniform distribution on the surface of a carbon carrier are synthesized. The peripheral electronic structure of Pt can be changed and the d-band center reduced by adding appropriate amounts of Co to the particles. Furthermore, the adsorption capacity of Pt on CO is reduced and the number of Pt active sites is increased, thereby improving the methanol oxidation performance and anti-poisoning ability of the PtCo/C nanoparticles.

References

1. J. Stejskal, M. Trchová. *Chem. Pap.,* 72 (2018) 7.
2. I.C. Gerber, P. Serp. *Chem. Rev.*, 12 (2019) 2.
3. L. Juárez-Marmolejo, S. Pérez-Rodríguez, M.M. Oca-Yemha, M. Palomar-Pardavé, M. Romero-Romo, M.J. Lázaro. *Int. J. Hydrogen Energy*, 44 (2019) 3.
4. S. Han, L. Ma, M. Gan, J. Shen, D. Wei, W. Zhan, X. Zhong. *Appl. Surf. Sci.*, 474 (2019) 30.
5. M. Luo, S. Guo. *Nat. Rev. Mater.*, 2 (2017) 11.
6. N. Han, K.R. Yang, Z. Lu, Y. Li, W. Xu, T. Gao, X. Sun. *Nat. commun.*, 9 (2018) 1.
7. C.F. Dickens, J.H. Montoya, A.R. Kulkarni, M. Bajdich, J.K. Nørskov. *Surf. Sci.*, 681 (2019) 12.
8. W. Zhang, Y. Hu, L. Ma, G. Zhu, Y. Wang, X. Xue, Z. Jin. *Adv. Sci.*, 5 (2018) 1.
9. R. Baronia, J. Goel, V. Kataria, S. Basu, S.K. Singhal. *Int. J. Hydrogen Energy*, 44 (2019) 20.
10. M.J. Lee, J.S. Kang, Y.S. Kang, D.Y. Chung, H. Shin, C.Y. Ahn, Y.E. Sung. *Acs Catal.*, 6 (2016) 4.
11. M.C. Moraes, G.G. Junco, T.F.M. Moreira, C.J.G. Pinheiro, P. Olivi, D. Profeti, L.P.R. Profeti. *J. Environ. Chem. Eng.*, 7 (2019) 1.
12. F. Jing, R. Sun, S. Wang, Y. Li, C. Yang, W. Ma, G. Sun. *Fuel Cells*, 19 (2019) 6.
13. F. Xie, L. Ma, M. Gan, H. He, L. Hu, M. Jiang, H. Zhang. *J. Power Sources*, 420 (2019) 783.
14. L. Wang, N.T. Nguyen, X. Huang, P. Schmuki, Y. Bi. *Adv. Funct. Mater.*, 27 (2018) 46.
15. H. Tan, J. Tang, J. Kim, Y.V. Kaneti, Y.M. Kang, Y. Sugahara, Y. Yamauchi. *J. Mater. Chem. A.*, 7 (2019) 4.
16. F. Wu, L. Zhang, J. Lai, R. Luque, W.R. Niu, G. Xu. *Nano Today*, 25 (2019) 10.
17. Z.A.C. Ramli, S.K. Kamarudin. *Nanoscale Res. Let.*, 13 (2018) 1.
18. J. Han, K. Kim, S. Kim, H. Lee, J. Kim, T. Ko, J.C. Lee. *J. Power Sources*, 448 (2020) 750.
19. L.M. Luo, W. Zhan, R.H. Zhang, D. Chen, Q.Y. Hu, Y.F. Guo, X.W. Zhou. *J. Power Sources*, 412 (2019) 142.
20. S.J. Zaidi, M. Bello, A. Al-Ahmed, A.B. Yousaf, M. Imran. *J. Electroanal. Chem.*, 794 (2017) 86.
21. Y.T. Pan, H. Yang. *Nano Today*, 1 (2020) 12.
22. J. Zhu, A.O. Elnabawy, Z. Lyu, M. Xie, E.A. Murray, Z. Chen, Y. Xia. *Materials Today*, (2019).
23. C. Kim, F. Dionigi, V. Beermann, X. Wang, T. Möller, P. Strasser. *Adv. Mater.*, 31 (2019) 31.
24. D.I. Potemkin, E.Y. Filatov, A.V. Zadesenets, V.A. Sobyanin. *Catal. Commun.*, 100 (2018) 1384.
25. T. Rajala, R. Kronberg, R. Backhouse, M.E.M. Buan, M. Tripathi, A. Zitolo, T. Kallio. *Appl. Catal. B-Environ.*, 265 (2020) 118582.
26. J.L. Yu, L.Y. Hao, B.B. Dong, F.H. Wang, S.A. Khan, Z. Li, S. Agathopoulos. *J. Mater. Chem. C.*, 7 (2019) 38.
27. T. Unmüssig, J. Melke, A. Fischer. *Phys. Chem. Chem. Phys.*, 21 (2019) 25.
28. Q. Liang, H. Jin, Z. Wang, Y. Xiong, S.R. Yuan, X. Zeng, S. Mu. *Nano Energy*, 57 (2019) 7.
29. S. Hanif, X. Shi, N. Iqbal, T. Noor, R. Anwar, A.M. Kannan. *Appl. Catal. B-Environ.*, *258* (2019) 11.
30. V. Johánek, A. Ostroverkh, R. Fiala. *Renew. energy*, 138 (2019) 4.
31. S. Kabir, D.J. Myers, N. Kariuki, J. Park, G. Wang, A. Baker, K.C. Neyerlin. *Acs Appl. Mater. Interf.*, 11(2019) 48.
32. J. Ying, J. Li, G. Jiang, Z.P. Cano, Z. Ma, C. Zhong, Z. Chen. *Appl. Catal. B-Environ.*, 225 (2018) 496.
33. Y.L. Zhang, J.L. Li, L. Zhao, X.L. Sui, Q.Y. Zhou, X.F. Gong, Z.B. Wang. *Electrochim. Acta*, 331 (2020) 135410.
34. C. Xie, Z. Niu, D. Kim, M. Li, P. Yang. *Chem. Rev.*, 12 (2019) 4683.
35. T.T. Huynh, H.Q. Pham, A. Nguyen, V.T.T. Phan, A.T.N. Mai, T.D. Nguyen. *Int. J. Hydrogen Energy*, 44 (2019) 37.
36. S. Hanif, X. Shi, N. Iqbal, T. Noor, R. Anwar, A.M. Kannan. *Appl. Catal. B-Environ.*, 258 (2019) 11.

37.   Chu.Y. Y, Wang. Z. B. Gu, Yin.G. P. *J. Power. Sources*, *195*(2010) 1799.
38. Guo. J.W, Zhao. T. S, Prabhuram. J, Chen. R, Wong. C. W. *Electrochim. Acta*, *51*(2005)754.
39. Fan. Y, Yang. Z, Huang. P, Zhang. X, Liu. Y. M. *Electrochim. Acta*, *105*(2013) 157.